Acta Crystallographica Section D
Biological Crystallography
ISSN 0907-4449

Structure of the C123S mutant of dienelactone hydrolase (DLH) bound with the PMS moiety of the protease inhibitor phenylmethylsulfonyl fluoride (PMSF)

Anna Robinson,[a]* Karen J. Edwards,[a] Paul D. Carr,[a] John D. Barton,[a] Gary D. Ewart[b] and David L. Ollis[a]

[a]Centre for Molecular Structure and Function, Research School of Chemistry, Australian National University, Canberra, ACT 0200, Australia, and [b]John Curtin School of Medical Research, Australian National University, Canberra, ACT 0200, Australia

Correspondence e-mail: anna.robinson@bigpond.com

Received 17 March 2000
Accepted 28 July 2000

PDB Reference: DLH C123S mutant–PMSF complex, 1ggv.

The structure of DLH (C123S) with PMS bound was solved to 2.5 Å resolution (R factor = 15.1%). PMSF in 2-propanol was delivered directly to crystals in drops and unexpectedly caused the crystals to dissolve. New crystals displaying a different morphology emerged within 2 h *in situ*, a phenomenon that appears to be described for the first time. The changed crystal form reflected altered crystal-packing arrangements elicited by structural changes to the DLH (C123S) molecule on binding inhibitor. The new unit cell remained in the $P2_12_12_1$ space group but possessed different dimensions. The structure showed that PMS binding in DLH (C123S) caused conformational changes in the active site and in four regions of the polypeptide chain that contain reverse turns. In the active site, residues with aromatic side chains were repositioned in an edge-to-face cluster around the PMS phenyl ring. Their redistribution prevented restabilization of the triad His202 side chain, which was disordered in electron-density maps. Movements of other residues in the active site were shown to be related to the four displaced regions of the polypeptide chain. Their implied synergy suggests that DLH may be able to accommodate and catalyse a range of compounds unrelated to the natural substrate owing to an inherent coordinated flexibility in its overall structure. Implications for mechanism and further engineering studies are discussed.

1. Introduction

Dienelactone hydrolase (DLH) is the third structural enzyme of the modified catechol *ortho*-cleavage pathway which is induced in soil-borne microorganisms in response to the uptake of otherwise toxic halogenated aromatic compounds (Schmidt & Knackmuss, 1980; Frantz & Chakrabarty, 1987; Frantz *et al.*, 1987; Ngai *et al.*, 1987; for reviews, see Schlömann, 1994; Harwood & Parales, 1996). Related pathways containing similar DLH enzymes have been identified in three operons from different microorganisms: the *clc* operon in *Pseudomonas putida* strains B13 and pAC27 (Dorn *et al.*, 1974; Chatterjee *et al.*, 1981), the *tcb* operon in *P. putida* p51 (P51) (van der Meer *et al.*, 1991) and the *tfd* operon in *Alcaligenes eutrophus* JMP134 (pJP4) (Don *et al.*, 1985; Perkins *et al.*, 1990). Although the three DLH enzymes are similar, their amino-acid sequences vary in parts and the substrates they catalyse possess different numbers and positions of chlorine substituents (for reviews, see van der Meer *et al.*, 1992; Schlömann, 1994).

The structure of DLH from the *clc* operon in *P. putida* (pAC27) was solved to 2.8 Å (Pathak *et al.*, 1988) and subsequently refined to 1.8 Å (Pathak & Ollis, 1990). The tertiary

structure of DLH was shown to be comprised of a centrally located β-sheet of eight strands surrounded by seven helices; a catalytic triad composed of the residues Cys123, His202 and Asp171 was found in the active site. The topological features of DLH form what was subsequently identified as an α/β hydrolase fold which typically contains an α/β sheet of eight β-strands connected by a variable number of α-helices (Ollis *et al.*, 1992). This fold has also been found in a large number of hydrolytic enzymes of widely differing phylogenetic origin and catalytic function (Ollis *et al.*, 1992; Hecht *et al.*, 1994; Wei *et al.*, 1995; Wang *et al.*, 1997; Kim *et al.*, 1997). The active sites of these enzymes have common features, including a catalytic triad, but the means by which they bind and hydrolyse substrates differ.

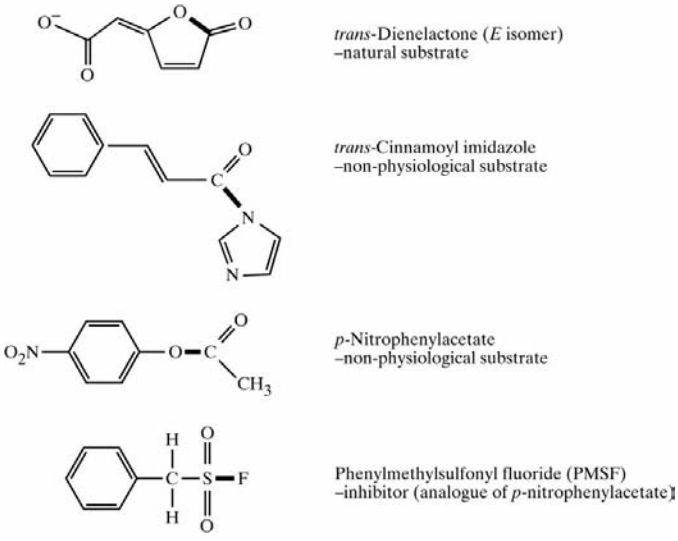

Figure 1
Structures of the natural substrate dienelactone compared with the non-physiological substrates *p*-nitrophenylacetate and *trans*-cinnamoyl imidazole as well as the inhibitor PMSF. The heavy line indicates the bond broken during catalysis.

Structural and computational analyses of wild-type DLH (wtDLH) supported the proposal that the side chain of the nucleophilic Cys123 rotates from an inactive to an active conformation on binding substrate (Pathak *et al.*, 1991; Cheah, Austin *et al.*, 1993; Beveridge & Ollis, 1995). However, when in the active conformation Cys123 appeared to oxidize in the X-ray beam (Pathak & Ollis, 1990). To overcome this problem, a C123S mutant was constructed in which the Ser123 hydroxyl group adopts a position equivalent to that of the activated Cys123 side chain (Pathak *et al.*, 1991). As the serine does not oxidize, the C123S mutant became the preferred model for crystallographic studies (Pathak *et al.*, 1991; Cheah, Ashley *et al.*, 1993; Cheah, Austin *et al.*, 1993).

Crystal structure analyses of the C123S mutant complexed with the isostructural substrate dienelactam identified residues involved in substrate binding. It was found that the carboxylate of the dienelactam interacts with two arginines, 81 and 206, which line the polar entry channel into the active site, while the ring moiety is directed towards a hydrophobic region formed by the predominantly aromatic side chains of residues Phe38, Tyr85, Trp88, Tyr145 and Phe173 (Cheah, Ashley *et al.*, 1993; Cheah, Austin *et al.*, 1993). Initially, this work was related to hydrolysis of substrate, as the C123S mutant appeared to have approximately 10–15% activity on the natural substrate (Pathak *et al.*, 1991). Subsequent work in our group has unexpectedly revealed that this activity arises from substrate isomerization rather than its hydrolysis (Walker *et al.*, 2000). Investigations into how this activity is derived in the C123S mutant are continuing.

In earlier kinetic studies, DLH and the C123S mutant were found to possess slow esterase activity on the non-physiological chromophoric ester substrate *p*-nitrophenylacetate and the synthetic peptide substrate *trans*-cinnamoyl imidazole (Pathak & Ollis, 1990; Pathak *et al.*, 1991; see Fig. 1). These compounds are structurally different from the natural substrate dienelactone and it was not clear how DLH could facilitate the hydrolysis of such unrelated compounds. It was particularly interesting to find that when the C123S mutant was reacted with *p*-nitrophenylacetate, a plot of the kinetic data showed an initial burst of phenolate formation. This result suggested that an acyl-enzyme intermediate was being formed during the reaction which might be observable in crystal structure analysis. We are interested

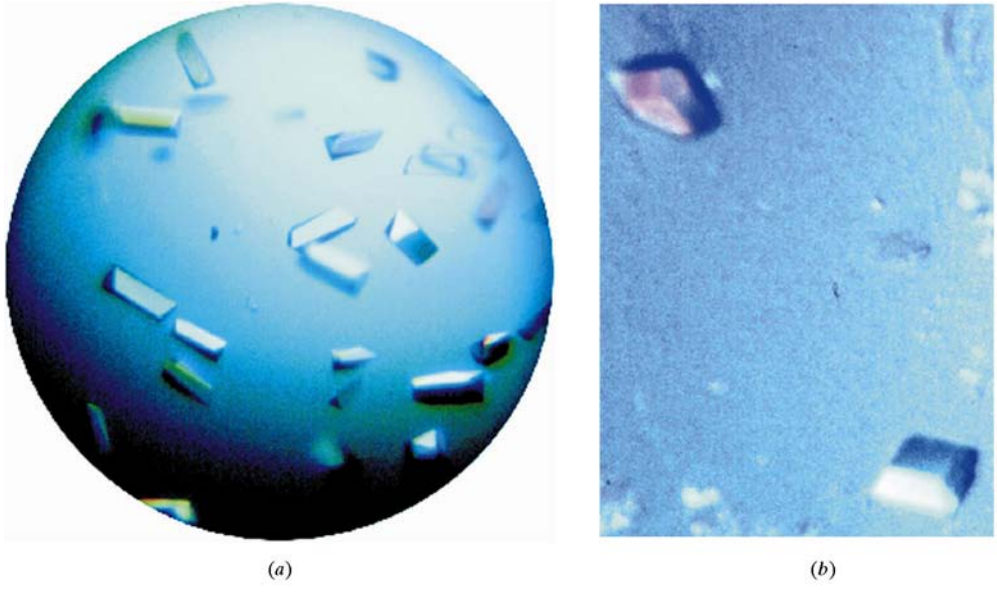

Figure 2
Crystals of DLH (C123S) before and after addition of PMSF in 2-propanol. C123S crystals (*a*) have dimensions of approximately 0.5 × 0.25 × 0.25 mm and show typical DLH morphology. C123S–PMS crystals (*b*) display the new square-shaped morphology and have dimensions of approximately 0.2 × 0.2 × 0.02 mm.

in determining how DLH is able to react and accommodate such a broad range of dissimilar substrates by identifying which residues in its structure are involved in their catalysis. As a first step, we sought an inhibited acyl-enzyme intermediate by reacting DLH (C123S) with phenylmethylsufonyl fluoride (PMSF). PMSF is a structural analogue of *p*-nitrophenylacetate (Fig. 1) and is also a serine protease/carboxylesterase inhibitor known to covalently bind with the serine of the Ser-His-Asp triad in the catalytic site (Gold, 1967; Wright *et al.*, 1969; Bott *et al.*, 1988; Chu *et al.*, 1995; Kim *et al.*, 1997). Here, we present the resulting 2.5 Å structure of DLH (C123S) with PMS bound in the active site (DLH–PMS) and compare the structure with the wild-type enzyme.

2. Experimental

2.1. Crystallization

Isolation, purification and crystallization of the mutant DLH (C123S) protein were carried out essentially as described previously (Pathak *et al.*, 1988). DLH (C123S) was crystallized from a 10 µl drop containing 7 µl of a 10 mg ml^{-1} protein solution mixed with 3 µl of 3 *M* phosphate (K^+/Na^+) at pH 6.3 equilibrated over 1.6–1.8 *M* phosphate at 291 K. 3 µl of a 50 or 100 m*M* solution of PMSF in 2-propanol was added directly to crystals in crystallizing drops on the cover slip (molar ratio of PMSF:enzyme $\simeq$ 100:1). This caused the crystals to dissolve, so the cover slip was replaced over the original well solution and the trays returned to 291 K. After approximately 2 h, new crystals showing a distinctively different morphology had re-formed in the drops. The crystals gradually increased in size over time and were large enough for X-ray analysis within 24 h. The new crystal morphology had square-shaped end faces and trapezoidal shaped sides (see Fig. 2). To check whether it was PMSF or alcohol solvent alone that was dissolving crystals, 3 µl of 2-propanol only was added to crystal drops. Crystals again dissolved, but in the absence of PMSF re-emerged displaying wtDLH morphology only; no new form crystals were observed. This identified 2-propanol as the causative agent of crystal dissolution and clearly showed that it was inhibitor binding to enzyme that was eliciting the changed crystal form.

2.2. Data collection

Diffraction data were collected at 277 K from one crystal of approximate dimensions 0.2 × 0.18 × 0.02 mm. The crystal was mounted in a quartz tube on a Rigaku RU-200 rotating-anode X-ray generator producing Cu $K\alpha$ radiation with power set at 50 kV and 100 mA. Data were recorded on a Rigaku R-AXIS IIC imaging-plate detector and processed, reduced, merged and scaled with software supplied by the manufacturer (Sato *et al.*, 1992). Crystals were rotated through 90° in 3° increments. Each frame was exposed to the X-ray beam for 15 min. The data-collection statistics are summarized in Table 1. The crystals formed in the space group $P2_12_12_1$, with unit-cell parameters a = 51.1, b = 51.9, c = 81.7 Å. The Matthews coefficient V_M (Matthews, 1968) was calculated as 2.13 Å^3 Da^{-1} for one molecule in the asymmetric unit.

Table 1
Data-collection statistics.

Space group	$P2_12_12_1$
Unit-cell parameters (Å)	a = 51.1, b = 51.9, c = 81.7
Resolution range (Å)	15.0–2.0
Completeness, overall (%)	78.3
Total reflections	30250
Unique reflections	12109
Highest resolution shell (Å)	2.0–2.09
R_{merge}† (%) with $F > 1\sigma(F)$ to 2.0 Å resolution	11.7

† $R_{merge} = \sum|I - \langle I\rangle|/\sum I$, where I is the observed intensity and $\langle I\rangle$ is the average intensity obtained from multiple observations of symmetry-related reflections.

2.3. Structure determination by molecular replacement

A rotation–translation function solution was obtained using the program *X-PLOR* v3.1 (Brünger, 1992). The 1.8 Å model of wtDLH (Pathak & Ollis, 1990) was used as the search model. Structure factors for the model Patterson map were calculated by placing the search model in a $P1$ cell with unit-cell dimensions 120 × 170 × 170 Å and $\alpha = \beta = \gamma = 90°$. The native Patterson map was calculated with 1667 reflections [$F > 2\sigma(F)$] in the resolution range 10–4 Å and vectors within a shell of radius 5–30 Å were used in subsequent calculations. The asymmetric unit of the rotation function (Rao *et al.*, 1980) was sampled at grid intervals of 2.5° and the 120 best solutions were filtered by the Patterson correlation refinement procedure. There was one prominent peak in the function, with angles θ_1 = 172.5, θ_2 = 37.5, θ_3 = 100.0°. This orientation was used in a translation search, which was carried out in the space group $P2_12_12_1$. The asymmetric unit for the translation search in fractional coordinates was x = 0–0.5, y = 0–0.5, z = 0–0.5 (Hirschfeld, 1968) with a step size of 0.02 fractional units. The highest peak was well separated from other solutions with T = 0.61 (the next largest peaks being T = 0.57 and T = 0.45). An R factor[1] of 34.7% was obtained after rigid-body refinement with 1667 reflections [$F > 2\sigma(F)$] in the resolution range 10–4 Å. An R factor of 33.6% was obtained after a second round of rigid-body refinement with 3855 reflections [$F > 2\sigma(F)$] in the resolution range 8–3 Å.

2.4. Structure refinement

Refinements were carried out using the program *X-PLOR* v3.1 (Brünger, 1992). Model building was carried out on an IRIS 4D/310 GVX workstation using the program *TOM* v3.0 (Israel & Chirino, 1994). $2F_o - F_c, \alpha_c$ and $F_o - F_c, \alpha_c$ electron-density maps were calculated to check the course of the refinement and manual adjustments were progressively made to the model. Omit electron-density maps were also calculated for selected residues to check that side chains had been modelled in the correct positions. Refinement was carried out in three stages and the progress of refinement is shown in

[1] $\sum||F_{obs}| - |F_{calc}||/\sum|F_{obs}| \times 100$, where summation is over all unique reflections.

Table 2
Progress of refinement.

All positional and *B*-factor refinements were taken to convergence. *B*-factor refinement = individual unrestrained temperature-factor refinement. All occupancies were set to unity and not refined.

Comments	*R* factor (%)
Stage 1. Resolution 8–3 Å, 3855 reflections	
Rigid-body refinement from MR	33.6
Positional refinement	23.4
Model building	
Stage 2. Resolution 8–2.5 Å, 6564 reflections	
Simulated annealing 3000–300 K	23.7
Grouped (isotropic restraints initially set to 15 Å^2) and individual *B*-factor refinement	22.0
Positional refinement	21.5
Model building, positional/*B*-factor/positional refinements	19.8
Stage 3. Resolution 7–2.5 Å, 6459 reflections	
Rebuild model, add 35 water molecules, positional/*B*-factor/positional refinements	17.4
Rebuild model, add 36 water molecules, positional/*B*-factor/positional refinements	15.0
Rebuild model, positional/*B*-factor/positional refinements	14.8
Rebuild model, delete 4 waters and remove side chain of His202, positional/*B*-factor/positional refinements	15.1

Table 3
Summary of final refinement statistics for C123S–PMS.

Resolution range (Å)	7.0–2.5
Number of reflections, $F > 2\sigma(F)$	6459
Completeness (%)	85.0
R factor (%)	15.1
Number of atoms (excluding H atoms)	
Total	2328
Protein	2254
Solvent	64
PMS	10
Average *B* factors (Å^2)	
Main chain	13.2
Side chain	14.2
Solvent	27.1
R.m.s. deviations of geometry from ideal values	
Bonds (Å)	0.010
Angles (°)	1.511
Dihedrals (°)	24.244
Impropers (°)	1.295

Table 2. Solvent molecules were included in the model if they appeared in both $2F_o - F_c$ and $F_o - F_c$ maps (with values above 2σ in the $F_o - F_c$ maps) and were between 2.8 and 3.5 Å from a potential hydrogen-bonding partner with appropriate stereochemistry. The PMS moiety of the compound 5*H*,8*H*-dibenzo(d,f)(1,2)oxathiocin-7,7-dioxide (located in the Cambridge Structural Database) was used as the initial model of the PMS ligand. Only the PMS portion of PMSF is required for incorporation into the structure, as the F atom is cleaved from the molecule during the binding reaction. The PMS molecule was unambiguously fitted into clearly defined density extending from Ser123 (Fig. 3) and the sulfate (SL) atom of the inhibitor was linked to the O (OG) atom of Ser123 creating a new residue, Pms123. Omit and difference electron density over residue His202 was clearly defined to the CB atom but was weak over the rest of the side chain at all stages of refinement. Attempts were made to fit His202 to the observed density in maps, but the side chain consistently drifted in subsequent refinement, clearly indicating that the residue was disordered. Refinement statistics are detailed in Table 3.

3. Results and discussion

3.1. New crystal form

Dissolution of DLH (C123S) crystals and their recrystallization in a different morphology after reaction with PMSF in 2-propanol (Fig. 2) was surprising and unexpected. The procedure described in §2 is routinely used for delivering inhibitor to enzymes in crystals and was adapted from that used by Kim (1994) to soak PMSF into carboxylesterase crystals. Kim reported that PMSF (dissolved in 1-propanol) reacting with the crystalline carboxylesterase enzyme caused no major change in either the external appearance of the crystals or enzyme structure; in contrast, the reaction of DLH (C123S) crystals with PMSF (dissolved in 2-propanol) caused significant changes in both. We demonstrated that crystal dissolution and rapid recrystallization occurred as the result of solvent effects. However, whether this was a consequence of having used the branched-chain rather than the linear isomer of propanol or was because of other reasons remains to be clarified.

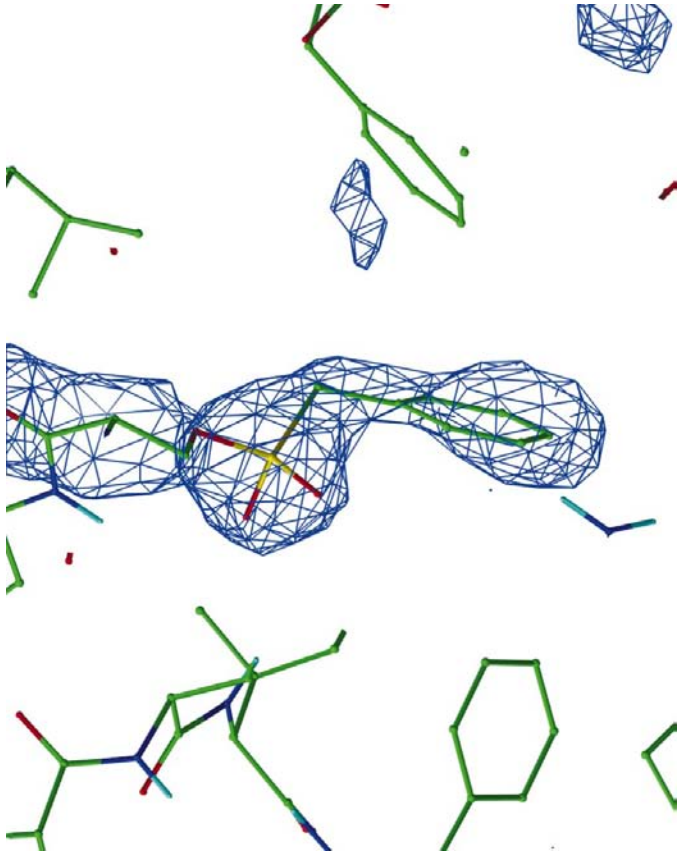

Figure 3
Omit density of the ligand phenylmethylsufonate (PMS) covalently bound to residue Ser123 of DLH (C123S). Density is contoured at 3σ.

3.2. Quality of the model

The $2F_o - F_c$ electron density contoured at the 1σ level was well defined and continuous for the main chain and 98% of side-chain residues in the model.

The structure was checked for stereochemical correctness using the program *PROCHECK* (Laskowski *et al.*, 1993). A Ramachandran plot[2] (Ramachandran & Sasisekharan, 1968) showed that out of all 190 non-glycine and non-proline residues, 178 (92.2%) were in the most favoured regions, 13 (6.7%) were in the additional allowed regions, Tyr145 (0.5%) was assigned to the generously allowed region and the new residue Pms123 (0.5%) was in the disallowed region. Residues Tyr145 and Cys/Ser123 are found in sharp turns of the polypeptide chain which provides the strained configurations of their side chains. Both turns are highly conserved in the α/β hydrolase-fold enzymes (Ollis *et al.*, 1992), the torsional constraint appearing to be essential for positioning of the catalytic residues.

B factors for the main chain and side chains ranged from 2.7 to 29.7 Å^2 and 2.0 to 42.9 Å^2, respectively. Temperature factors for solvent molecules ranged from 5.0 to 59.0 Å^2. Regions of the molecule exhibiting higher than average temperature factors for both main-chain and side-chain values involved residues 74–78, 82–83, 107–113, 150–155, 168–175, 199–203 and 207–210. These groups of residues represent the more flexible parts of the molecule: either loops, some of which incorporate turns interspersed between secondary-structural elements, or residues located at surface areas of the molecule with unconstrained side chains extending into solvent. Above average thermal motion is not unexpected in these regions.

3.3. Overall structure

The topology of C123S–PMS retains the characteristic conformation of an α/β hydrolase fold (Fig. 4) and essential features of the molecule are as previously described (Pathak & Ollis, 1990; Pathak *et al.*, 1991). In forming the new residue Pms123, the PMS ligand bound synergistically in the amphipathic active site (Fig. 5). The Pms123 OG atom is positioned 2.7 Å from the main-chain N atom of Leu124 and potential hydrogen bonds exist between main-chain atoms of Pms123, Tyr144 and Gly126. The 123 sulfate O atoms are directed towards the region defined as the oxyanion hole (Cheah, Ashley *et al.*, 1993), but only OD1 is within hydrogen-bonding distance (3.3 Å) of Ile37 N; OD2 makes no potential stabilizing contacts at all. The Pms123 aromatic ring is directed towards the hydrophobic region of the active site and makes van der Waals contacts with nearby residues Tyr85, Trp88 and Phe173.

A van der Waals interaction also exists between the Pms123 ring and Arg81 CZ (distance of 3.5 Å). This is an unusual interaction caused by a >1.0 Å lateral movement of the Arg81 side chain in towards the active site and over the Pms123 ring, the guanidinium group concomitantly rotating 27° so that the NH1 and NH2 groups appear to straddle the 123 ring edge (see Fig. 6). The extent of this displacement is difficult to explain, as the residue could have been stabilized in a more accommodating location away from the Pms123 ring. It seems possible that a favourable energy contribution might be provided by induction of an NH_2 amino–π hydrogen bond or interaction. The relationship satisfies criteria that have been determined for amino–aromatic interactions in that it occurs between a bound ligand and enzyme; the positive charged amino groups pack within 3.4–6 Å of the centroid of an aromatic ring; the interaction serves to orient the arginine side chain without interfering with its ability to form hydrogen bonds elsewhere; the geometric reconfiguration aligns the (δ^+) Arg81 terminal amino groups with the (δ^-) π-electrons of the Pms123 aromatic ring, although the Arg–aromatic configuration is different to the offset planar arrangement above the carbon ring described previously (Levitt & Perutz, 1988; Flocco & Mowbray, 1994; Mitchell *et al.*, 1994; for a review, see Scrutton & Raine, 1996).

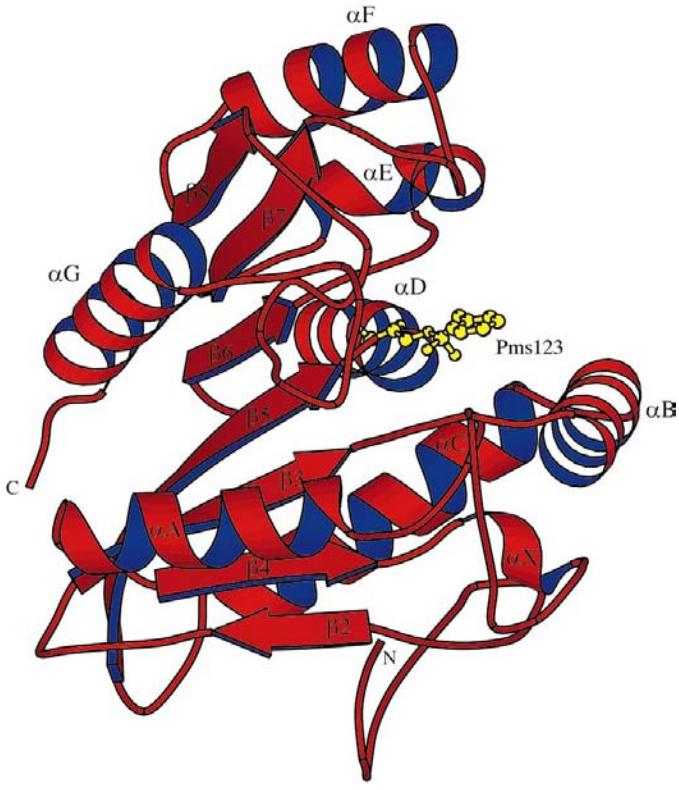

Figure 4
A schematic diagram of DLH (C123S) with PMS bound (*MOLSCRIPT*; Kraulis, 1991) Secondary-structural elements are labelled to correspond with the labelling scheme first used for wtDLH (Pathak *et al.*, 1988). The *DSSP* program (Kabsch & Sander, 1983) used in this study omitted the β1 sheet shown in wtDLH and assigned an additional α-helix, labelled αX to avoid interrupting the alphabetical sequence. The active site is defined by a series of interconnecting loops and the αB helix is in a solvent-exposed cavity. The new residue Pms123 is depicted as a ball-and-stick model and is coloured yellow.

[2] Supplementary materials are available from the IUCr electronic archive (Reference: gr2044). Services for accessing these data are described at the back of the journal.

Table 4
Potential intermolecular hydrogen-bond interactions (2.8–3.5 Å) between symmetry-related molecules.

(*a*) C123S–PMS. In this model, there did not appear to be potential intermolecule hydrogen-bond interactions between molecules related by the $-x+\frac{1}{2}, -y, z+\frac{1}{2}$ symmetry operator. This was not unexpected, as the residues Gln76 and Glu78 in wtDLH which previously formed symmetry-related contacts in this group occur in parts of the molecule that underwent significant change in the present structure (*cf.* Table 4*b*).

Contact residue–symmetry-related residue	Symmetry operator	Distance (Å)
His14 (NE2)–Ser22 (OG)	$-x, y+\frac{1}{2}, -z+\frac{1}{2}$	3.21
Arg81 (NE)–Glu222 (OE1)		3.33
Arg81 (NH2)–Glu222 (OE2)		3.50
Water-mediated contacts		
Ser22 (OG)–Wat267 (O)		3.16
Ser22 (O)–Wat266 (O)		3.26
Pro23 (O)–Wat267 (O)		3.06
Trp50 (NE1)–Wat288 (O)		3.09
Pro69 (O)–Wat238 (O)		2.90
Ser215 (OG)–Wat280 (O)		3.48
His161 (NE2)–Gln180 (NE2)	$x+\frac{1}{2}, -y+\frac{1}{2}, -z$	3.27
His161 (NE2)–Glu184 (OE2)		3.34

(*b*) wtDLH (adapted from Pathak & Ollis, 1990).

Contact residue–symmetry-related residue	Symmetry operator	Distance (Å)
Gln9 (NE2)–Gln76(O)	$-x+\frac{1}{2}, -y, z+\frac{1}{2}$	3.03
Gln9 (OE1)–Glu78 (N)		2.84
Glu4 (OE2)†–His161 (ND1)	$-x, y+\frac{1}{2}, -z+\frac{1}{2}$	3.38
Gly5 (O)–Gln193 (NE2)		3.46
Ser22 (OG)–Ala188 (O)		3.04
Arg81 (NH2)–Glu222 (OE2)	$x+\frac{1}{2}, -y+\frac{1}{2}, -z$	3.00
Arg81 (NE)–Glu222 (OE2)		3.26
Arg81 (NE)–Glu222 (OE1)		2.55
Glu82 (OE1)–Arg223 (NH2)		3.18
Tyr85 (OH)–Glu222 (OE2)		2.79
His172 (NE2)†–Asn221 (OD1)		3.42

† In C123S–PMS, these side chains are disordered and only partically observed.

3.4. Intermolecular crystal contacts

Four symmetry-related molecules of C123S–PMS are located in the unit cell and there is one molecule in the asymmetric unit. Each molecule makes five direct protein–protein hydrogen-bond contacts to two symmetry-related neighbours (Table 4*a*). Additional lattice contacts are mediated by six solvent molecules which stabilize the packing of the crystal. Many intermolecular non-bonded van der Waals contacts (3.2–3.9 Å) to neighbouring molecules are also observed.

Intermolecular contacts determined for wtDLH are shown in Table 4(*b*). Significant differences exist in both the number and positions of symmetry-related contacts even though the two structures remain very similar. However, most of the changes involve those parts of the molecule that have undergone conformational change and the new relationships are therefore not unexpected. One particular feature is that two symmetry-related contacts between Arg81 NH1 and NH2 and Glu222 OE in wtDLH are retained in C123S–PMS, despite significant movement of Arg81 in the active site. This suggests that crystallization may proceed *via* the formation of a dimer of two DLH molecules linked by hyrogen bonds between Arg81 and Glu222.

3.5. Comparison of C123S–PMS and wtDLH structures

The overall structures of C123S–PMS and wtDLH are almost the same, as shown in the superimposition of their C^{α} backbones (Fig. 7). The similarity between the two models is also reflected by the low r.m.s. deviations for equivalent C^{α} atoms and main-chain atoms, calculated to be 0.41 and 0.42 Å, respectively. Secondary structure in C123S–PMS was essentially unperturbed and reflects the stability of the tertiary α/β hydrolase fold. Only the active site and four segments of the polypeptide chain (peptide *A*, residues Gln9, Ser10, Tyr11, Asp12; peptide *B*, residues Asp74, Pro75, Gln76; peptide *C*,

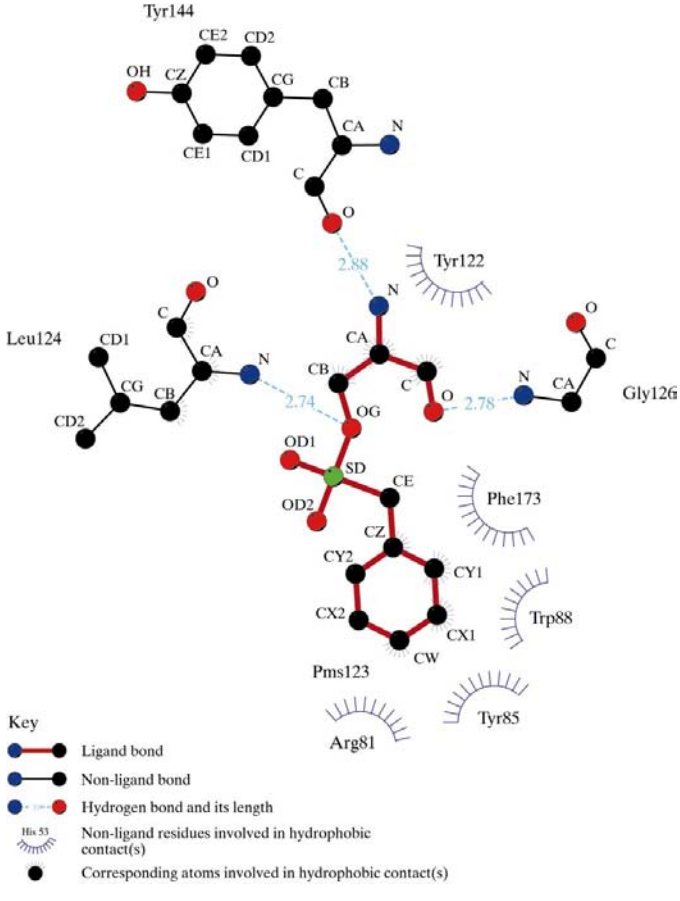

Figure 5
A two-dimensional *LIGPLOT* (Wallace *et al.*, 1994) representation of the Pms123 residue showing potential hydrogen-bonding partners and non-bonded interactions. The amphipathic nature of the residue is demonstrated by the segregated regions of hydrophilic and hydrophobic contacts. Potential hydrogen bonds surround the Pms O atoms and main-chain polar groups, while the hydrophobic contacts are predominantly clustered around the aromatic ring. The potential hydrogen-bonded contact between Ile37 and Pms123 OD1 (see text) is not shown.

Glu170, Asp171, His172, Phe173, Val174, Pro175, Ala176; peptide *D*, Glu199 and immediate surrounding region) differed by more than 1.0 Å. These changes represent a very small alteration in the DLH structure overall.

PMS binding caused displacement of mainly hydrophobic residues (or those with hydrophobic moieties) in the active site, with the exclusion of His202 which could not be determined (Fig. 6). Side chains of Phe38, Phe173, Tyr145 and Tyr85 show the largest primary displacements, while the movement of the Ile37 and Val147 side chains appears to be secondary, arising only from disrupted contacts with the Phe38 and Phe173 aromatic rings, respectively. Only a slight adjustment of the Phe38 ring occurred [from 0.62 Å (CD2) to 0.72 Å (CZ)], but the movement displaced the adjacent Ile37 side chain [0.51 Å (CG1) to 1.03 Å (CD1)] away from the interactive space between the Pms123 and Phe38 aromatic rings. Movement of the Phe173 side chain from its original location was much greater [from 1.2 Å (CA) to more than 2.0 Å (CE1 and CZ)], which disrupted a previously stabilizing contact with the side chain of Val147. The terminal group of Val147 rotated approximately 56° away from the active site, increasing the distance between the atoms of the two side chains from 0.91 to nearly 3.0 Å. The increased distances between the Phe38/Ile37 and Phe173/Val147 side chains was somewhat surprising given the favourable interactions between the two groups in their original location. However, molecular-mechanics calculations indicate that interactions between aromatic rings are stronger than those between an aromatic ring and other hydrophobic side chains (Hunter *et al.*, 1991), suggesting that rearrangements observed in C123S–PMS involve attractive forces of aromatic networks.

The aromatic rings have undergone a geometric as well as spatial rearrangement, stabilizing in an edge-to-face orientation in the active site. This configuration has been shown to be the energetically favourable geometry of phenyl-ring interactions in protein-folding studies (Warme & Morgan, 1978; Singh & Thornton, 1985; Burley & Petsko, 1985; Hunter *et al.*, 1991). Energy considerations may also account for the (conventionally interpreted as) unfavourable interactions of aromatic rings with nearby side chains. The CW and CX atoms of residue Pms123 are only 2.9 Å from the NH2 atom of residue Arg81 and 2.6 Å from the hydroxyl group of residue Tyr85, respectively; the ring CD2 atom of residue Phe173 is positioned only 3.3 Å from the OD2 atom of the triad residue Asp171. These distances are close for a non-hydrogen bonded interaction but may represent polar–aromatic interactions which contribute weak but significant energy terms through a mixture of hydrogen bonds and a more favoured geometry between residues (Burley & Petsko, 1985, 1986; Jones & Chapman, 1995; Parkinson *et al.*, 1996; for reviews, see Burley & Petsko, 1988; Jeffrey, 1995; Scrutton & Raine, 1996; Nishio *et al.*, 1998).

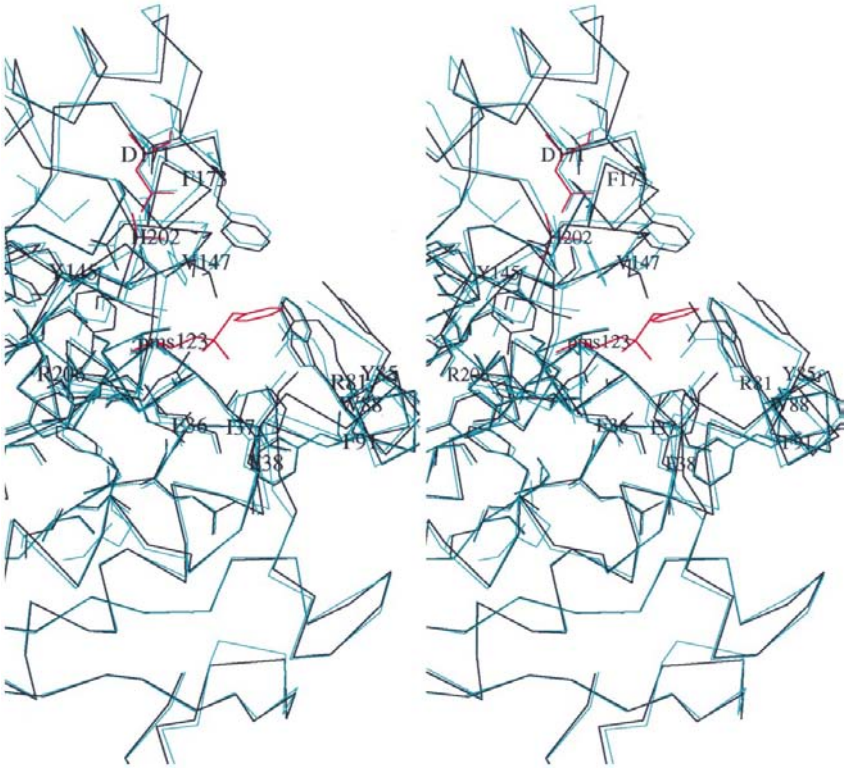

Figure 6
Stereoview (*MOLSCRIPT*; Kraulis, 1991) showing the active site of C123S–PMS (black) overlaying the active site of wtDLH (cyan). Triad residues of C123S–PMS are shown in red (His202 is shown to the CB atom only, as the side chain was removed during structural refinement).

3.6. Coordinated restructuring

It was interesting to find that displacements in peptides *A*, *B*, *C* and *D* could also be explained in terms of the changes brought about by PMS binding. Movement in these regions appears to occur essentially because of changes in positions of only residues Tyr85/Arg81 and Phe173 in the active site. The movement of Tyr85 away from Pms123 disrupted a stabilizing interaction with the Arg81 side chain, whose movement induced the concomitant displacement of residues Asp74, Pro75, Gln76 (peptide *B*) in towards the active site. Displacement of peptide *B* appears to influence movement of peptide *A* through the disruption of previously observed symmetry-related contacts between Gln9 and Gln76. Movement of Phe173 in towards the active site caused rearrangement of the main and side chains of nearby residues in peptide *C* (residues 170–176). Their displacement fully exposed this region to solvent and the increased side-chain mobility thus introduced allowed the Glu170 side chain (NE1 and OE atoms) to make a close approach to the aliphatic portion of the Glu199 side chain. This was in turn displaced, causing destabilization of peptide *D* (the region around Glu199). The interrelation of DLH active-site

movements and those in peptides *A*, *B*, *C* and *D* suggests that they are not independent events. In fact, the implied synergy is similar to that identified in trypsin, chymotrypsin, elastase (Hedstrom, 1996 and cited references) and dihydrofolate reductase (reviewed in Benkovic, 1998), where a relationship between the active-site residues and remote peptides has been shown to influence reaction rates.

It should be pointed out that although that the relationship between peptides *A* and *B* involves intermolecular contacts, the overall changes could not have been caused by altered molecular-packing arrangements alone. A cause-and-effect relationship can clearly be established from the inhibitor-bound active site to the external peptides, but not the reverse.

3.7. His202 destabilization

What remains unclear is why the His202 side chain is destabilized in the C123S–PMS structure and whether it is an integral part of the restructuring. In the resting state, His202 is stabilized by a hydrogen-bonded network with triad partners Asp171 and Ser123 (Pathak *et al.*, 1991). His202 movement probably occurs on binding the PMS inhibitor as it is observed to rotate when the hydrogen-bonded interaction is disrupted in the DLH (E171N) mutant (Cheah, Austin *et al.*, 1993) and also when the Cys123 side chain is modified (John Barton, unpublished work). A rotating triad His has also been observed in other structures of enzymes with PMS bound, resulting in geometrically rearranged contacts between triad residues and bound inhibitor (Wright *et al.*, 1969; Chu *et al.*, 1995; Kim *et al.*, 1997). Interpretations presented by these researchers suggest the His movement may be an integral part of the catalytic mechanism (Chu *et al.*, 1995) whose function may be to stabilize the ES intermediate (Kim *et al.*, 1997).

It seemed possible that the same reasoning could be applied to DLH, so an attempt was made to manually rotate the His202 side chain into a more stabilized position in the C123S–PMS model. However, when rotated to one side the imidazole ring made a close approach (2.3–3.2 Å) to the Phe173 aromatic ring and the ring atoms of Pms123 (<3.0 Å); in the other direction, the NE2 atom could be suitably positioned within 3.4 Å of both the Pms123 OG and SD atoms, the NE1 atom a distance of 2.6 Å (originally 2.6 Å) and 3.2 Å (originally 3.3 Å) from the respective OD1 and OD2 atoms of residue Asp171. This provided the expected stabilizing interaction between His202 and a PMS sulfonyl O atom, except that the 202 NE2 atom made unfavourable contacts (<3.5 Å distance) with the CE atom of the Tyr145 aromatic ring which appears to prevent its stabilization in this orientation.

Tyr145 has moved 1.34 Å in towards Glu36 in C123S–PMS, which is difficult to understand. No nearby residues sterically encroach into the region and while Ramachandran analysis shows residue Tyr145 is in the generously allowed region, the values of the φ and ψ angles are 35 and 65.6° in the present model, which compare well with previous values of 40 and 59° in the wild-type enzyme (Pathak & Ollis, 1990). Attempts to relocate the Tyr145 side chain into a more accommodating position were unsuccessful, possibly because of torsional constraints, suggesting that Tyr145 movement must also be integral to the overall restructuring.

For efficient catalysis to occur, we would expect His202 to be positioned in an appropriate orientation for stabilizing the intermediate and protonating the leaving group, as has been observed in other transition-state analogues. Instead, its destabilization suggests that progressive synergistic conformational adjustments must occur after binding substrate which facilitate repositioning of the His202 side chain prior to triad-mediated chemistry. Such pre-organization of active-site residues is not unknown and has also been implicated in lysozyme (Warshel & Levitt, 1976), acetylcholine esterase (also an α/β hydrolase enzyme; Sussman *et al.*, 1991) and staphylococcal nuclease as well as orotidine-5-monophosphate decarboxylase (reviewed in Cannon & Benkovic, 1998).

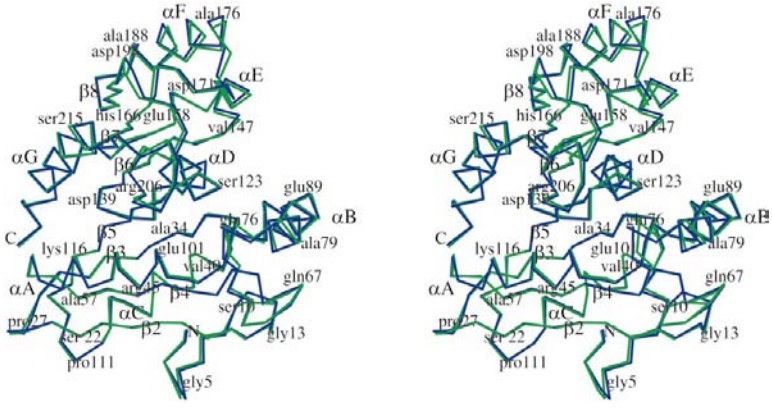

Figure 7
Stereoview of the superimposed α-carbon traces of C123S–PMS (green) and wtDLH (dark blue) structures. Secondary structures are labelled and selected residues are identified.

4. Concluding remarks

The structure of C123S–PMS has revealed some significant insights into DLH activity. Our model suggests that dissimilar substrates can be catalysed in DLH because of an intrinsic flexibility existing in only small regions of its polypeptide chain. The flexibility appears to enable the enzyme to undergo a coordinated restructuring without compromising the stability of its tertiary fold.

The capacity of DLH to be spatially accommodating seems to be the means by which a wide range of molecules gain access to the active site and are able to react with the nucleophile. The ensuing slow rates of catalysis on non-physiological substrates in DLH (C123S) are probably a consequence of the concomitant disorganization of triad residues which are not optimally aligned.

It seems likely that the flexibility also exists in wtDLH because, firstly, crystal structure analysis of the two molecules in the resting state shows that their overall conformations are virtually the same

(Pathak *et al.*, 1991); secondly, 123 is the only mutated residue and regions of the polypeptide chain that confer flexibility are identical in both enzymes and not directly influenced by the nucleophile; lastly, given that wtDLH is also active on *p*-nitrophenylacetate and *trans*-cinnamoyl imidazole, it is difficult to see how these bulkier substrates can be fitted in wtDLH without conformational adjustment occurring in the manner observed in the C123S–PMS model.

This work will facilitate future mutagenesis and protein design studies aimed at engineering improved activity of DLH on non-natural substrates.

We thank Professor Bi, Institute of Biophysics, Academia Sinica, China for providing parameter and topology files for the PMS molecule, and David Hockless for providing the structure coordinates for the PMS ligand. Thanks also to the ANU Supercomputer Facility, ANU for use of their Fujitsu VP2000 or VPP2200 computers. Particular gratitude is extended to Greg Petsko (Brandeis, USA) and Chris Easton (RSC) for reading the manuscript and valuable comments. Anna Robinson and John Barton were the recipients of Australian National University Postgraduate Scholarships.

References

Benkovic, S. J. (1998). *J. Phys. Org. Chem.* **11**, 508–511.
Beveridge, A. J. & Ollis, D. L. (1995). *Protein Eng.* **8**, 135–142.
Bott, R., Ultsch, M., Kossiakoff, A., Graycar, T., Katz, B. & Power, S. (1988). *J. Biol. Chem.* **263**(16), 7895–7906.
Brünger, A. T. (1992). *X-PLOR Version* 3.1. *A System for X-ray Crystallography and NMR.* Yale University, Connecticut, USA.
Burley, S. K. & Petsko, G. A. (1985). *Science*, **229**, 23–28.
Burley, S. K. & Petsko, G. A. (1986). *FEBS Lett.* **203**, 139–143.
Burley, S. K. & Petsko, G. A. (1988). *Adv. Protein Chem.* **39**, 125–189.
Cannon, W. R. & Benkovic, S. J. (1998). *J. Biol. Chem.* **273**(41), 26257–26260.
Chatterjee, D. K., Kellogg, S. T., Hamada, S. & Chakrabarty, A. M. (1981). *J. Bacteriol.* **146**(2), 639–646.
Cheah, E., Ashley, G. W., Gary, J. & Ollis, D. L. (1993). *Proteins Struct. Funct. Genet.* **16**, 64–78.
Cheah, E., Austin, C., Ashley, G. W. & Ollis, D. (1993). *Protein Eng.* **6**(6), 575–583.
Chu, N.-M., Chao, Y. & Bi, R.-C. (1995). *Protein Eng.* **8**(3), 211–215.
Don, R. H., Weightman, A. J., Knackmuss, H.-J. & Timmis, K. N. (1985). *J. Bacteriol.* **161**(1), 85–90.
Dorn, E., Hellwig, M., Reinecke, W. & Knackmuss, H.-J. (1974). *Arch. Microbiol.* **99**, 61–70.
Flocco, M. M. & Mowbray, S. L. (1994). *J. Mol. Biol.* **235**, 709–717.
Frantz, B. & Chakrabarty, A. M. (1987). *Proc. Natl Acad. Sci. USA*, **84**, 4460–4464.
Frantz, B., Ngai, K., Chatterjee, D. K., Ornston, L. N. & Chakrabarty, A. M. (1987). *J. Bacteriol.* **169**(2), 704–709.
Gold, A. M. (1967). *Methods Enzymol.* **11**, 706–711.
Harwood, C. S. & Parales, R. E. (1996). *Annu. Rev. Microbiol.* **50**, 553–590.
Hecht, H.-J., Sobek, H., Haag, T., Pfeifer, O. & van Pee, K.-H. (1994). *Struct. Biol.* **1**(8), 532–537.
Hedstrom, L. (1996). *Biol. Chem.* **377**, 465–470.
Hirschfeld, F. L. (1968). *Acta Cryst.* A**24**, 301–311.
Hunter, C. A., Singh, J. & Thornton, J. M. (1991). *J. Mol. Biol.* **218**, 837–846.
Israel, M. & Chirino, A. J. (1994). *TOM/FRODO. A Molecular Modelling Program for the IRIS, Version* 3.0. Alberta: Caltech.
Jeffrey, G. A. (1995). *Cryst. Rev.* **4**, 213–259.
Jones, G. B. & Chapman, B. J. (1995). *Synthesis*, **1**, 475–497.
Kabsch, W. & Sander, C. (1983). *Biopolymers*, **22**, 2577–2637.
Kim, K. K. (1994). PhD thesis, Seoul National University, Seoul, Korea.
Kim, K. K., Song, H. K., Dong, H. S., Hwang, K. Y., Choe, S., Yoo, O. J. & Suh, S. W. (1997). *Structure*, **5**, 1571–1584.
Kraulis, P. J. (1991). *J. Appl. Cryst.* **24**, 946–950.
Laskowski, R. A., MacArthur, M. W., Moss, D. S. & Thornton, J. M. (1993). *J. Appl. Cryst.* **26**, 283–291.
Levitt, M. & Perutz, M. F. (1988). *J. Mol. Biol.* **201**, 751–754.
Matthews, B. W. (1968). *J. Mol. Biol.* **33**, 491–497.
Meer, J. R. van der, de Vos, W. M., Harayama, S. & Zender, A. J. B. (1992). *Microbiol. Rev.* **56**(4), 677–694.
Meer, J. R. van der, Zender, A. J. B., Eggen, R. I. K. & de Vos, W. M. (1991). *J. Bacteriol.* **173**(8), 2425–2434.
Mitchell, J. B. O., Nandi, C. L., McDonald, I. K., Thornton, J. M. & Price, S. L. (1994). *J. Mol. Biol.* **239**, 315–331.
Ngai, K.-L., Schlömann, M., Knackmuss, H.-J. & Ornston, L. N. (1987). *J. Bacteriol.* **16**9(2), 699–703.
Nishio, M., Hirota, M. & Umezawa, Y. (1998). Editors. *The CH/π Interaction. Evidence, Nature and Consequences.* New York: Wiley–VCH.
Ollis, D. L., Cheah, E., Cygler, M., Dijkstra, B., Frolow, F., Franken, S. M., Harel, M., Remington, S. J., Silman, I., Schrag, J., Sussman, J. L., Verschueren, K. H. G. & Goldman, A. (1992). *Protein Eng.* **5**(3), 197–211.
Parkinson, G., Gunasekera, A., Vojtechovsky, J., Zhang, X., Kunkel, T. A., Berman, H. & Ebright, R. H. (1996). *Nature Struct. Biol.* **3**(10), 837–841.
Pathak, D., Ashley, G. & Ollis, D. (1991). *Proteins Struct. Funct. Genet.* **9**, 267–279.
Pathak, D., Ngai, K. L. & Ollis, D. (1988). *J. Mol. Biol.* **204**, 435–445.
Pathak, D. & Ollis, D. (1990). *J. Mol. Biol.* **214**, 497–525.
Perkins, E. J., Gordon, M. P., Caceres, O. & Lurquin, P. F. (1990). *J. Bacteriol.* **172**(5), 2351–2359.
Ramachandran, G. N. & Sasisekharan, V. (1968). *Adv. Protein Chem.* **23**, 283–437.
Rao, S. N., Jih, J.-H. & Hartsuck, J. A. (1980). *Acta Cryst.* A**36**, 878–884.
Sato, M., Yamamoto, M., Katasumi, I., Katsube, Y., Tanaka, N. & Higashi, T. (1992). *J. Appl. Cryst.* **25**, 348–357.
Schlömann, M. (1994). *Biodegradation*, **5**, 301–321.
Schmidt, E. & Knackmuss, H.-J. (1980). *Biochem. J.* **192**, 339–347.
Scrutton, N. S. & Raine, A. R. C. (1996). *Biochem. J.* **319**, 1–6.
Singh, J. & Thornton, J. M. (1985). *FEBS Lett.* **191**(1), 1–6.
Sussman, J. L., Harel, M., Frolow, F., Oefner, C., Goldman, A., Toker, L. & Silman, I. (1991). *Science*, **253**, 872–879.
Walker, I., Easton, C. J. & Ollis, D. L. (2000). *Chem. Commun.* pp. 671–672.
Wallace, A. C., Laskowski, R. A. & Thornton, J. M. (1994). *LIGPLOT Version* 1.0, *A Program to Produce Automated Representations of Protein–Ligand Interactions.* Biomolecular Structure and Modelling Unit, Department of Biochemistry and Molecular Biology, University College, Gower Street, London WC1E 6BT, England.
Wang, X., Wang, C.-S., Tang, J., Dyda, F. & Zhang, Z. C. (1997). *Structure*, **5**, 1209–1218.
Warme, P. K. & Morgan, R. S. (1978). *J. Mol. Biol.* **118**, 289–304.
Warshel, A. & Levitt, M. (1976). *J. Mol. Biol.* **103**, 227–249.
Wei, Y., Schottel, J. L., Derewenda, U., Swenson, L., Patkar, S. & Derewenda, Z. S. (1995). *Struct. Biol.* **2**(3), 218–223.
Wright, C. S., Alden, R. A. & Kraut, J. (1969). *Nature (London)*, **221**, 235–242.